Chemical Physics Letters 477 (2009) 319–324

Contents lists available at ScienceDirect

Chemical Physics Letters

journal homepage: www.elsevier.com/locate/cplett

A new route to dual fluorescence: Spectroscopic properties of the valence tautomers of a 3-(2*H*)-isoquinolinone derivative

Ian M. Craig [a], Hieu M. Duong [a,b,1], Fred Wudl [a,b,2], Benjamin J. Schwartz [a,*]

[a] University of California, Los Angeles Department of Chemistry and Biochemistry, Los Angeles, CA 90095-1569, USA
[b] University of California, Los Angeles Institute for Advanced Materials, Los Angeles, CA 90095-1569, USA

ARTICLE INFO

Article history:
Received 6 April 2009
In final form 9 July 2009
Available online 12 July 2009

ABSTRACT

The isoquinolinone derivative 2-methyl-1,4-diphenylbenzo[g]isoquinolin-3(2*H*)-one (MDP-BIQ) shows dual fluorescence emission with band positions and intensities that depend sensitively on the solvent. We show that this behavior arises from the fact that MDP-BIQ has two valence tautomers, one aromatic and one conjugated but non-aromatic, each of which are separately fluorescent. The aromatic tautomer, which has significant zwitterionic character, is stabilized by trace amounts of hydrogen-bond donors or Lewis acids. The relatively high fluorescence quantum yield of the aromatic tautomer (0.127 versus 2.4×10^{-3} for the non-aromatic tautomer) makes this and similar molecules outstanding candidates for use in sensors and other optoelectronic applications.

1. Introduction

The electronic properties of aromatic polyacenes (e.g., anthracene, tetracene, pentacene) have received a great deal of recent attention due to the potential application of their molecular crystals in optoelectronic devices [1]. One of the key obstacles to the practical use of these materials in applications lies in the fact that the larger polyacenes are unstable; even pentacene is at best marginally stable in the presence of air [2]. This has prompted synthetic chemists to add heteroatoms to polyacenes in an effort both to tune their electronic properties and to improve their chemical stability. In this paper, we explore the electronic structure of one such polyacene derivative, 2-methyl-1,4-diphenylbenzo[g]isoquinolin-3(2*H*)-one (MDP-BIQ; see Fig. 1A (inset), below, for chemical structure). Most strikingly, we find that MDP-BIQ (**I**) exhibits dual fluorescence in solution: following photoexcitation, the molecule emits light in distinct green and red fluorescence bands.

The phenomenon of dual fluorescence, in which an excited molecular chromophore emits from two different excited states in apparent violation of Kasha's rule [3], was first discovered by Albert Weller in 1956 in salicylic acid and assigned to excited-state intramolecular proton transfer (ESIPT) [4], in which emission can occur from both the normal and proton-transferred tautomeric forms of the excited-state [5,6]. The phenomenon was later observed in *p*-N,N-dimethylamino-benzonitrile (DMABN) by Lippert et al. [7], and later assigned by Rotkiewicz et al. [8] to the formation of two different excited states: a local (Franck–Condon) excited state, and a relaxed charge-separated state stabilized by twisting around the amine–phenyl bond. This stabilization of an internally charge-separated excited state by large-amplitude intramolecular twisting has been dubbed 'twisted intramolecular charge transfer' (TICT), and has since been observed in a wide variety of molecular species [9,10].

In addition to TICT, nearly a dozen other mechanisms for dual fluorescence have been described in the literature [11]. Two of these mechanisms share important similarities with the phenomena reported here. The first is ESIPT, in which the dual emission comes from distinct excited-state tautomers as observed in molecules such as 3-hydroxyflavone [12,13]. The second is dual amplified spontaneous emission, which has been observed from H-bonding induced charge transfer in coumarin-like dye molecules [14,15]. We note that ESIPT and other dual fluorescent molecules can be used as sensitive probes of their local environment [16], including in applications such as *in situ* pH sensors [17] and monitoring the curing of adhesives [18]. Dual fluorescent molecules also have a key advantage over traditional fluorescence probes: conventional fluorescent tags can only be either on or off, but a dual fluorescent probe can be 'on' in either of the two emission states, providing not only a sensitive measure of the local environment but also a means to determine whether the fluorescent probe is truly 'off' or is simply absent due to some type of photo- or chemical-degradation process [16,19].

It is clear from its molecular structure that **I** cannot fall into the TICT or ESIPT class of dual fluorescent molecules because it has no coordinate around which a large-amplitude twist could stabilize a charge-separated excited state and because it contains no protons

* Corresponding author.
E-mail address: schwartz@chem.ucla.edu (B.J. Schwartz).
[1] Present address: ZPower, Inc., 4765 Calle Quetzal, Camarillo, CA 93012, USA.
[2] Present address: University of California, Santa Barbara, Department of Chemistry and Biochemistry, Santa Barbara, CA 93106-9510, USA.

0009-2614/$ - see front matter © 2009 Elsevier B.V. All rights reserved.
doi:10.1016/j.cplett.2009.07.041

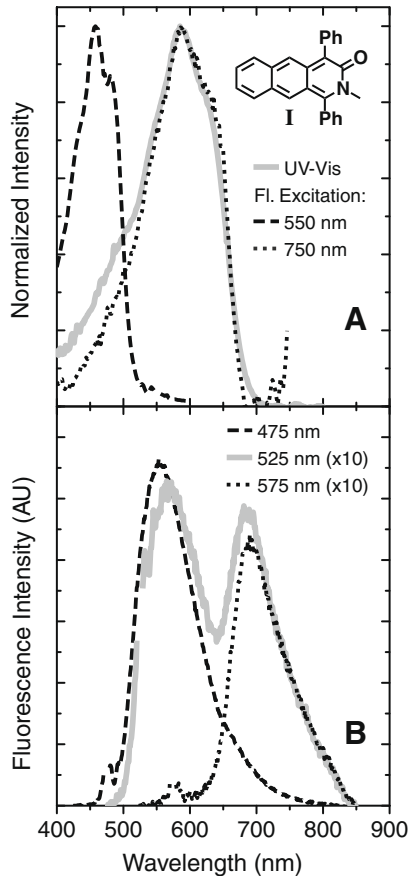

Fig. 1. Absorption and emission properties of MDP-BIQ (**I**, shown in inset) in undistilled chloroform. (A) Absorption (solid gray curve) and fluorescence excitation spectra of the 550 nm (dashed curve) and 750 nm (dotted curve) emission peaks. (B) Fluorescence spectra of **I** exciting at 475 nm (dashed curve), 525 nm (solid gray curve), and 575 nm (dotted curve), scaled by the incident light intensity and sample OD at the excitation wavelength. The emission spectra for 525 and 575 nm have been scaled by an additional factor of 10 for ease of comparison. (Data gaps in the emission are from the removal of peaks due to scattered light from the excitation source.)

that could transfer in the excited state. We find that the dual fluorescence properties of **I** share aspects of both ESIPT and the hydrogen-bonding induced charge transfer seen in the coumarins [15], but with the notable difference that the induced shifts in the electronic structure of this molecule occur in the ground electronic state. This offers the opportunity to use molecules like **I** not only in applications for dual fluorescent probes, but also as indicators as well as in the myriad potential optoelectronic applications associated with the polyacenes.

2. Experimental and theoretical methods

The synthesis of 2-methyl-1,4-diphenylbenzo[g]isoquinolin-3(2*H*)-one was originally reported some time ago [20], but recent improvements in the synthetic scheme [21,22] have made it possible to produce large quantities of high-purity material with minimal synthetic work-up. For this study, samples were characterized by single-crystal X-ray crystallography, FTIR, and ^{1}H and ^{13}C NMR to verify structure and purity [22].

To eliminate photobleaching of the molecule during spectroscopic measurements, all solvents were degassed using the freeze–pump–thaw method to remove dissolved oxygen [23] and then stored under nitrogen. All solutions, unless otherwise specified, were prepared in an inert-atmosphere (nitrogen) glove box.

Table 1
Absorption and emission maxima of both the neutral (**I**, red-emitting) and charge transfer (**II**, green-emitting) forms of MDP-BIQ in various solvents (undistilled). The absorption max in each solvent was determined using fluorescence excitation spectroscopy. The absorption max values for vacuum are those calculated for TM-BIQ for the protonated (**V**) and unprotonated forms (**III**).

Solvent	Absorption max		Emission max		Lifetime	
	II	**I**	**II**	**I**	**II**	**I**
DMSO[a]	370 nm	597 nm	435 nm	715 nm	2.3 ns	370 ps
CCl_4	450 nm	560 nm	563 nm	670 nm	–	–
Chloroform	460 nm	593 nm	562 nm	715 nm	2.3 ns	370 ps
Acetonitrile	470 nm	593 nm	575 nm	715 nm	–	–
TFA[b]	475 nm	n/a	555 nm	n/a	11.3 ns	n/a
Toluene	480 nm	617 nm	555 nm	670 nm	830 ps	260 ps
Cyclohexane	502 nm	590 nm	605 nm	720 nm	–	–
Vacuum	505 nm[c]	611 nm[d]	–	–	–	–

[a] Dimethylsulfoxide.
[b] Trifluoroacetic acid.
[c] Calculated value for **V**.
[d] Calculated value for **III**.

Absorption and emission spectra were taken in quartz fluorescence cuvettes with Teflon-sealed screw caps. Solutions exposed to ambient conditions irreversibly photobleached in 2–3 h, but those protected from air lasted indefinitely.

Absorption spectra were taken on a Perkin–Elmer Lambda-25 spectrometer, and most steady-state emission and fluorescence excitation spectra were taken on a JY Horiba Tau3 spectrometer. Because a large portion of the red emission band of **I** lies beyond the 800 nm detection limit of the Tau3, the emission measurement for the fluorescence quantum yield of the red-emitting state, as well as the emission of the corresponding standard, was collected using a HeNe laser excitation source and an Ocean Optics USB1000 fiber optic spectrometer with a NIR grating and detector designed for use from 600 to 1275 nm. The spectra measured on this instrument were corrected via calibration with a 2800 K blackbody tungsten–halogen lamp with a constant-current power supply. The quantum yield standard used for the red emission was buckminsterfullerene (C_{60}, QY = 2.4×10^{-3}) in toluene [24], and the standard employed for the green emission was sodium fluorescein in 0.1 M aqueous NaOH (QY = 0.95) [25].

Emission lifetime measurements were taken using an Axis Photonique streak camera in conjunction with a 1 kHz femtosecond laser excitation source, with the different emission colors separated using Schott colored glass filters; the ultrafast laser system and streak camera operation are described in detail elsewhere [26,27]. For both the red and green emission, the dynamic fluorescence fit well to single-exponential decays whose lifetimes are quoted in Table 1, below.

Electronic structure calculations were performed with GAMESS (version 12 JAN 2009 (R1)) [28,29]. The geometry optimization was done using density functional theory (DFT) with the B3LYP functional, 6-31+G(d,p) basis set, and the default convergence criteria. The first two singlet excited states were calculated using time-dependent density functional theory (TDDFT) using the same functional and basis set as for the geometry optimization. The absorption spectrum and Kohn–Sham density of states (DOS) data were extracted from the output files using GaussSum [30].

3. Results and discussion

Fig. 1 shows the absorption (solid gray curve, panel A), fluorescence excitation spectra (dotted and dashed curve, panel A), and emission spectra (panel B) of **I** in a degassed chloroform solution. The absorption spectrum shows only a single band, which peaks at ~580 nm and has shoulders associated with vibronic side bands

as commonly seen in conjugated molecules. In contrast, the emission spectrum of **I** clearly shows two bands, a green one peaked at ~562 nm that lies almost entirely beneath the main absorption band, and a Stokes-shifted red band peaked at ~670 nm that has roughly the Franck–Condon mirror image of the main absorption band.

Unlike TICT or ESIPT, Fig. 1B shows that the relative intensity of the two emission bands changes with excitation wavelength: for sufficiently red excitation (dashed curve) the green emission band disappears, and vice-versa for green excitation (dotted curve) while excitation at intermediate wavelengths leads to emission from both bands (solid gray curve). Fluorescence excitation spectra, collected at the peak wavelengths of both the green (dashed curve) and red (dotted curve) emission bands are shown in Fig. 1A along with the absorbance spectrum (solid gray curve). The excitation spectra strongly suggest that the two emission bands arise from independent electronic excitations, even though only a single molecule is present in solution. Time-resolved measurements also indicate different fluorescence lifetimes for the two emission bands: as summarized in Table 1, in all the solvents for which we did measurements, we found that the lifetime of the red emission band is much shorter than that of the green band. The lifetime of the green band is also much longer in the polar solvents dimethylsulfoxide (DMSO) and chloroform than in the non-polar solvent toluene. In trifluoroacetic acid (TFA), the red emission band is completely quenched and the lifetime of the green emission is ~5 times longer than that in DMSO or chloroform.

The two peaks seen in the fluorescence excitation spectra in Fig. 1A cannot be assigned to two electronic transitions within the same molecule for two reasons. First, the positions of these excitation peaks are not what is typically seen for electronic excited states of the same molecule. Unless there is something particularly unusual about the electronic structure of **I**, the two excitation and emission bands are much closer together in energy than what would be expected for the lowest few singlet excited states of a conjugated molecule, and the absorption and emission of the green peak is much more intense than what would be expected for a triplet state. Second, the lifetimes are not consistent with emission from separate S_2 and S_1 states: one would expect at least some internal conversion between the S_2 and S_1 states (Kasha's rule) [3], which is not consistent with the longer lifetime and higher quantum yield of the green emission.

To gain a better understanding of the nature of the dual fluorescence from **I**, we measured the absorption and emission properties of this molecule in a variety of solvent environments; the peak positions of the green and red excitation and emission bands and their fluorescence lifetimes are also summarized in Table 1. Interestingly, the position of the red emission band is relatively insensitive to the choice of solvent, whereas the green emission band undergoes dramatic shifts in position in different solvents: the green emission band shifts over 170 nm (0.80 eV) between dimethylsulfoxide (DMSO) and cyclohexane, while the red band shifts only 50 nm (0.13 eV) over the entire range of solvents studied. Table 1 also makes it clear that the relative positions of the green and red emission bands do not correlate well with the solvent polarity (e.g., the relative peak positions are vastly different not only in non-polar solvents such as CCl_4 and cyclohexane but also in polar solvents such as DMSO and acetonitrile (CH_3CN)). Finally, as mentioned above, in trifluoroacetic acid (TFA), the red excitation and emission peaks are unobservable: only the green absorption and emission bands are present.

Although the dual fluorescence we measured in the various solvents was quite reproducible, we found that when working with solutions in $CHCl_3$ the relative quantum yields of the green and red emission bands changed if the solutions had not been properly degassed. Since chloroform can be photochemically decomposed in the presence of oxygen to form phosgene ($COCl_2$), chlorine (Cl_2) and hydrochloric acid (HCl) [23], we suspected that one of the photochemical byproducts was affecting the electronic structure of MDP-BIQ. In Fig. 2, we compare the emission properties of **I** in chloroform that had only been degassed to the emission properties in chloroform that had been refluxed over anhydrous calcium chloride and then distilled under argon to remove any inhibitors, residual water, decomposition products, or dissolved oxygen. The spectra have been scaled by the sample optical density and the intensity of the fluorimeter lamp at the indicated excitation wavelengths. The intensity of the green emission band is reduced in the distilled chloroform by a factor of 8, while the intensity of the red emission band remains essentially unchanged (inset). If we let the freshly-distilled chloroform sit for several days before use, we found that the fluorescence once again becomes dominated by the green emission peak.

The fact that the intensity of the green emission in $CHCl_3$ varies with the presence of impurities, which include HCl, in combination with the fact that only the green emission is present in TFA, suggests that the presence of acid is somehow correlated with the green emission. We intentionally added several different protic acids to solutions of **I** in several solvents, and found that the intensity of the green emission peak increased greatly upon the addition of even trace amounts of acid: the increase in green emission with acid addition appeared to be stoichiometric. We also found that the addition of tiny amounts of ethanol or other protic but non-acidic solvents also had the same effect, suggesting that the presence of hydrogen-bonding impurities – not just acidic impurities – is what is important in controlling the intensity of the green emission.

To explain this observation, we note that the chemical structure of **I**, although highly conjugated, is not aromatic. In the presence of an H-bond donor, such as TFA, HCl or ethanol, the carbonyl group can become an enolate stabilized by the H-bond donor. This allows the N atom on the ring to take on a (partially) positive charge, producing an aromatic zwitterion, as illustrated in Scheme 1. In this scheme, the driving force to produce the charge-separated zwitterion **II** is the acquisition of aromaticity; thus, even a relatively weak interaction, such as the H-bond from ethanol, is sufficient to produce the aromatic zwitterion from the non-aromatic 'normal' form of the molecule. Thus, the dual emission of MDP-BIQ is explained

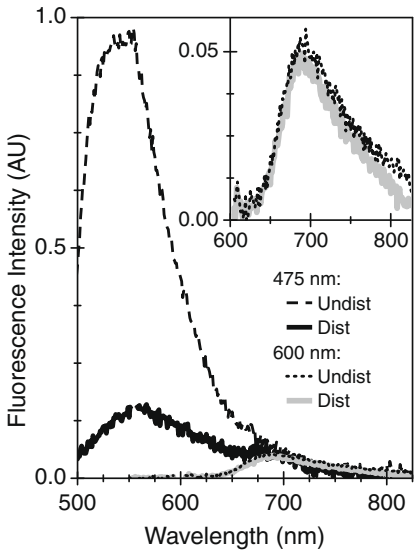

Fig. 2. Fluorescence of **I** in as-received (dashed curves) and re-distilled (solid curves) chloroform following excitation at both 475 and 600 nm. The inset shows an expansion of the 700 nm emission peak. The spectra presented are scaled by the incident light intensity and sample OD at the excitation wavelength.

two distinct tautomers whose relative populations can be reversibly controlled.

Fig. 3 also shows that it takes quite a large amount of acid to have a noticeable effect on the absorption spectrum of MDP-BIQ, but only trace amounts of impurities are sufficient to affect the emission spectrum, as is seen in Fig. 2. This is a direct result of the fact that the aromatic tautomer **II** has a much higher emission quantum yield than tautomer **I**. Because of the overlap of the zwitterionic and neutral tautomer absorption and emission bands, we only were able to reliably measure the quantum yield of tautomer [redacted]

by the fact that this [redacted] e has 2 valence [redacted]

[redacted] ding impuri- [redacted] tautomerization of the molecule, we [redacted] the electronic properties of the three [redacted] lin-3(2*H*)-one (TM-BIQ [redacted] boron trifluori [redacted] and a proton (**V**) attached to the oxygen, which [redacted] logues for MDP-BIQ tautomer **II**. Table 1 [redacted] we considered, we found that the [redacted] almost completely between the HOMO and LUMO [redacted] orbitals, suggesting a pure one-electron $S_0 \rightarrow S_1$ transition, as shown in Fig. 5A. The calculated position of the absorption transition for structure **III** is in excellent agreement with the experimental absorption spectrum of MDP-BIQ in distilled toluene, where we expect the molecular structure to correspond entirely with tauto- [redacted] absorption to the blue, again in accord with the experimental spectrum of MDP-BIQ tautomer **II** in TFA. The calculations also show that structures **V** and **IV** have nearly identical HOMO–LUMO gaps, consistent with our experimental observations that the identity of the constituent attached to the oxygen does not matter as long as it provides sufficient stabilization to convert the ‘normal’ form of the molecule to the aromatic zwitterionic form and thus widen the absorption gap.

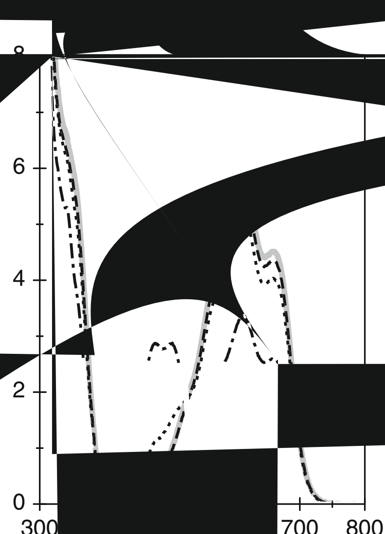

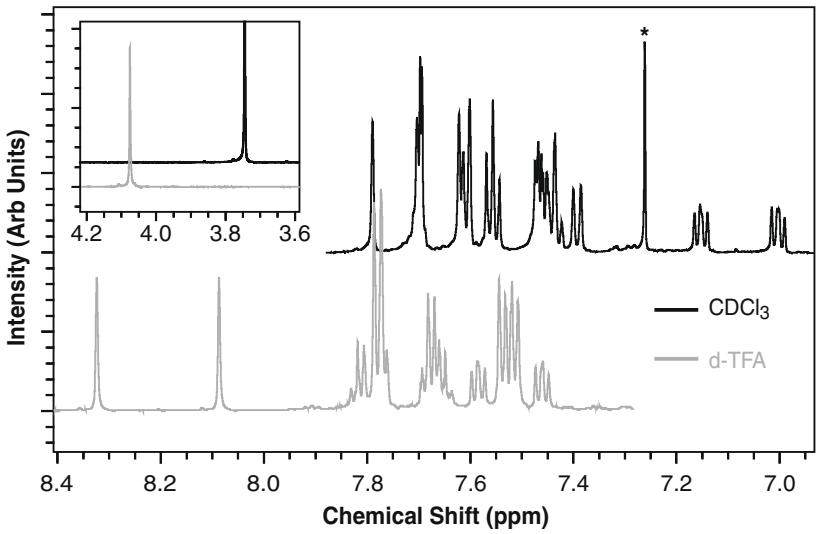

Fig. 4. ^{1}H NMR spectra of MDP-BIQ in $CDCl_3$ (black) and deuterated trifluoroacetic acid (d-TFA) (gray) in the aromatic region [31] with the $CDCl_3$ spectra vertically offset for clarity and the N-methyl region shown in the inset. The starred peak is the solvent peak from trace amounts of $CHCl_3$.

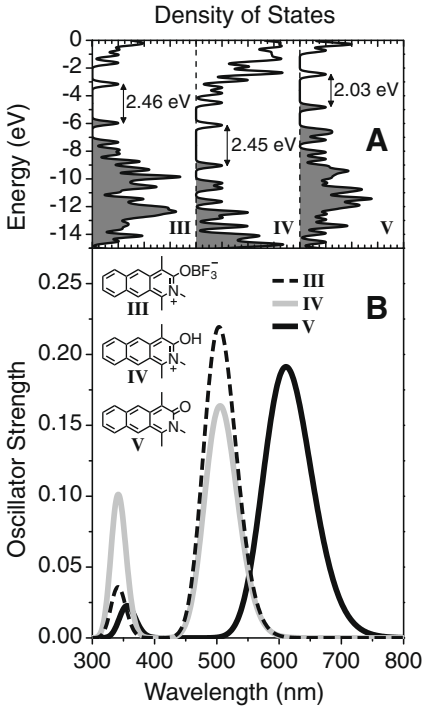

Fig. 5. TD-DFT-calculated density of Kohn–Sham states (A) and absorption spectrum (B) of gas phase 1,2,4-trimethylbenzo[g]isoquinolin-3(2*H*)-one in its neutral form (**III**) and with either a proton (**V**) or the neutral Lewis acid boron trifluoride (**IV**) attached to the oxygen. In panel A, filled states are shaded in gray and empty states in white. The peaks in both panels have been broadened with a 0.3-eV Gaussian for ease of comparison to experiment.

4. Conclusions

In summary, we have shown that the dual fluorescence of the heteroatom-modified polyacene MDP-BIQ results from the presence of a zwitterionic, aromatic, valence tautomer form of the molecule that can be produced by interaction with weak H-bond donors or electron acceptors. This provides a different mechanism for dual fluorescence than is commonly seen in molecules that undergo TICT or ESIPT. The two tautomers of MDP-BIQ are distinct chemical moieties, explaining the two different emission bands with different peak positions, quantum yields and fluorescence lifetimes. The driving force to gain aromaticity is strong enough that the relative populations of the two tautomers can be easily shifted by trace amounts of Lewis acids or H-bond donors. The extreme sensitivity of the emission to even tiny of amounts of relatively weak H-bond donors such as ethanol offers exciting possibilities for the use of molecules like MDP-BIQ as indicators for a wide variety of trace impurities. Moreover, the ease with which MDP-BIQ can be controllably switched between its two tautomers suggests a variety of optoelectronic applications: if crystals of isoquinolinones have similar electronic properties as their parent polyacenes, the ability to switch the band gap of the material by simple exposure to HCl or NH_3 vapor (or other solid-permeable H-bond or electron donors and acceptors) may provide a new route to easily chemically-tunable optoelectronic devices.

Acknowledgements

The authors would like to acknowledge the support of NSF grant CHE–0527015 and ONR contract N-00014-04-1-0410. NMR data was taken on equipment purchased on NSF equipment grants CHE–9974928 and CHE–0116853. The authors also thank Colin Carver, Bob Taylor, and the UCLA Molecular Instrumentation Facility for their help with the NMR data, and UCLA Academic Technology Services for access to the UCLA Hoffman2 Beowulf cluster used for the GAMESS calculations.

References

[1] J.E. Anthony, Chem. Rev. 106 (12) (2006) 5028.
[2] M. Bendikov, F. Wudl, D.F. Perepichka, Chem. Rev. 104 (11) (2004) 4891.
[3] M. Kasha, Discuss. Faraday Soc. 9 (1950) 14.
[4] A. Weller, Z. Elektrochem. 60 (9–10) (1956) 1144.
[5] S.J. Formosinho, L.G. Arnaut, J. Photochem. Photobiol. A: Chem. 75 (1) (1993) 21.
[6] A.S. Klymchenko, A.R. Demchenko, in: Fluorescence Spectroscopy, Methods in Enzymology, vol. 450, Elsevier Academic Press Inc., 2008, p. 37.
[7] E. Lippert, W. Lüder, F. Moll, W. Nägele, H. Boos, H. Prigge, I. Seibold-Blankenstein, Angew. Chem. 73 (21) (1961) 695.
[8] K. Rotkiewicz, K.H. Grellmann, Z.R. Grabowski, Chem. Phys. Lett. 19 (3) (1973) 315.
[9] Z.R. Grabowski, K. Rotkiewicz, W. Rettig, Chem. Rev. 103 (10) (2003) 3899.
[10] V.V. Volchkov, B.M. Uzhinov, High Energy Chem. 42 (3) (2008) 153.
[11] Y. Inoue, P. Jiang, E. Tsukada, T. Wada, H. Shimizu, A. Tai, M. Ishikawa, J. Am. Chem. Soc. 124 (24) (2002) 6942.

[12] D.A. Yushchenko, V.V. Shvadchak, A.S. Klymchenko, G. Duportail, Y. Mély, V.G. Pivovarenko, New J. Chem. 30 (2006) 774.
[13] D.A. Yushchenko, V.V. Shvadchak, M.D. Bilokin', A.S. Klymchenko, G. Duportail, Y. Mély, V.G. Pivovarenko, Photochem. Photobiol. Sci. 5 (11) (2006) 1038.
[14] R.W. Yip, Y.X. Wen, J. Photochem. Photobiol. A: Chem. 54 (2) (1990) 263.
[15] R.W. Yip, Y.X. Wen, Can. J. Chem. – Revue Can. Chim. 69 (9) (1991) 1413.
[16] A.P. Demchenko, FEBS Lett. 580 (12) (2006) 2951.
[17] F. Galindo, J. Becerril, M. Isabel Burguete, S.V. Luis, L. Vigara, Tetrahedron Lett. 45 (8) (2004) 1659.
[18] K. Hakala, R. Vatanparast, S. Li, C. Peinado, P. Bosch, F. Catalina, H. Lemmetyinen, Macromolecules 33 (16) (2000) 5954.
[19] A. Demchenko, Lab on A Chip 5 (11) (2005) 1210.
[20] D.W. Jones, R.L. Wife, J. Chem. Soc.: Perkin Trans. 1 (1972) 2722.
[21] F. Wudl, K. Starkey, H. Duong, Abstracts Papers Am. Chem. Soc. 221 (Part 2) (2001) 423.
[22] H.M. Duong, Ph.D. Thesis, University of California, Los Angeles, Los Angeles, CA, 2003.
[23] W.L.F. Armarego, D.D. Perrin, Purification of Laboratory Chemicals, fourth edn., Butterworth, Heinemann, Oxford, 1997.
[24] B. Ma, Y.P. Sun, J. Chem. Soc.: Perkin Trans. 2 10 (10) (1996) 2157.
[25] J.R. Lakowicz, Principles of Fluorescence Spectroscopy, second edn., KluwerAcademic/Plenum Publishers, 1999.
[26] I.B. Martini, A.D. Smith, B.J. Schwartz, Phys. Rev. B: Condens. Matter Mater. Phys. 69 (3) (2004) 035204.
[27] T.Q. Nguyen, I.B. Martini, J. Liu, B.J. Schwartz, J. Phys. Chem. B 104 (2) (2000) 237.
[28] M.W. Schmidt et al., J. Comput. Chem. 14 (11) (1993) 1347.
[29] M.S. Gordon, M.W. Schmidt, Theory and Applications of Computational Chemistry: The First Forty Years, Theory and Applications of Computational Chemistry: The First Forty Years, Chapter 41: Advances in Electronic Structure Theory: GAMESS a Decade Later, Elsevier Academic Press Inc., Amsterdam, 2005.
[30] N.M. O'Boyle, A.L. Tenderholt, K.M. Langner, J. Comput. Chem. 29 (5) (2008) 839.
[31] ^{1}H NMR ($CDCl_3$, 500 MHz) δ 3.74 (s, 3H), 7.00 (t, 1H), 7.15 (t, 1H), 7.39 (d, 1H), 7.45 (m, 4H), 7.56 (t, 2H), 7.61 (m, 3H), 7.70 (m, 3H), 7.79 (s, 1H) ppm; ^{1}H NMR (d-TFA, 600 MHz) δ 4.08 (s, 3H), 7.46 (t, 1H), 7.51 (d, 2H), 7.53 (d, 2H), 7.58 (t, 1H), 7.66 (m, 3H), 7.79 (m, 6H), 8.09 (s, 1H), 8.32 (s, 1H) ppm; ^{13}C NMR ($CDCl_3$, 500 MHz) δ 37.3, 116.2, 117.6, 120.5, 124.4, 127.3, 128.0, 128.3, 128.7, 129.1, 129.2, 129.2, 129.5, 129.6, 130.3, 131.5, 133.7, 136.3, 136.8, 137.1, 153.8, 158.2 ppm; ^{13}C NMR (d-TFA, 600 MHz) δ 41.6, 120.3, 124.5, 125.5, 129.8, 130.1, 130.2, 130.6, 131.4, 131.6, 132.0, 132.3, 132.5, 132.9, 133.9, 134.3, 135.0, 135.5, 136.7, 140.8, 149.2 ppm.
[32] N.S. Isaacs, Physical Organic Chemistry, Wiley, 1987.